

Manuscript Title: Projection patterns of corticofugal neurons associated with vibrissa movement

Authors: Ken-ichi Shibata^{1,2}, Takuma Tanaka³, Hiroyuki Hioki^{1,4}, Takahiro Furuta^{1,2}

¹Department of Morphological Brain Science, Graduate School of Medicine, Kyoto University, Kyoto 606-8501, Japan

²Department of Oral Anatomy and Neurobiology, Graduate School of Dentistry, Osaka University, Suita 565-0871, Japan

³Faculty of Data Science, Shiga University, Hikone 522-8522, Japan

⁴Department of Cell Biology and Neuroscience, Graduate School of Medicine, Juntendo University, Tokyo 113-8421, Japan

Author contributions: K.S. performed the experiments, analyzed the data, and wrote the manuscript. T.T. analyzed the data and helped write the manuscript. H.H. produced the plasmid and helped write the manuscript. T.F. designed and supervised the experiments and helped write the manuscript. All authors commented on the manuscript.

Corresponding author: Correspondence and material requests should be addressed to Dr. Takahiro Furuta, Department of Oral Anatomy and Neurobiology, Graduate School of Dentistry, Osaka University, Suita 565-0871, Japan. E-mail: furuta@dent.osaka-u.ac.jp.

Number of figures and tables: 9 figures and 2 tables.

Number of words for Abstract, Significance Statement, Introduction, and Discussion: 119 words for Abstract, 56 words for Significance Statement, 427 words for Introduction, and 994 words for Discussion.

Acknowledgements: We thank Dr. Kei Oyama and Professor Ken-ichiro Tsutsui (Tohoku University) for help with the electroporation technique.

Conflict of Interest: Authors report no conflict of interest.

Funding sources: This work was supported by Grants-in-Aid for Scientific Research from Ministry of Education, Culture, Sports, Science, and Technology (16K16123 to T.T., 15H01430, 16H04663, 16H01426, 17K19451 to H.H., and 23135519, 24500409, 15H04266 to T.F.), and partially by the program for Brain Mapping by Integrated Neurotechnologies for Disease Studies (Brain/MINDS) from the Japan Agency for Medical Research and development, AMED.

Abstract

Rodents actively whisk their vibrissae, which, when they come in contact with surrounding objects, enables rodents to gather spatial information about the environment. Cortical motor command of whisking is crucial for the control of vibrissa movement. Using awake and head-fixed rats, we investigated the correlations between axonal projection patterns and firing properties in identified layer 5 neurons in the motor cortex, which are associated with vibrissa movement. We found that cortical neurons that sent axons to the brainstem fired preferentially during large-amplitude vibrissae movements and that corticocallosal neurons exhibited a high firing rate during small vibrissa movements or during a quiet state. The differences between these two corticofugal circuits may be related to the mechanisms of motor-associated information processing.

Key words: whisker; single cell electroporation; pyramidal tract neuron; intratelencephalic neuron

Significance Statement

The contents of cortical motor commands and the pathways that they take are two important questions in neuroscience. Previous studies in rodents reported that motor cortex neurons exhibit variable activity patterns during whisking behavior. We combined physiological and morphological analyses of single neurons to provide more detail for understanding the neural circuit related to motor control.

Introduction

Rodents use vibrissae, which are long hairs on the sides of their faces, as tactile sensors that help them gather spatial information about the environment (Diamond et al., 2008; Kleinfeld and Deschênes, 2011). Specifically, rodents can obtain tactile descriptions of texture, shape, and position by actively moving their vibrissae to touch objects (Welker, 1964; Mitchinson et al., 2011). In a typical vibrissal movement pattern, which is called “whisking”, rodents repeatedly sweep their vibrissae back and forth such that they contact any objects located in the space surrounding the head of the animal. During exploratory behavior, the speed and amplitude of whisking are precisely adjusted by the vibrissal motor system depending on the situation and chosen behavioral strategies (Towal and Hartmann, 2006; Mitchinson et al., 2007; Grant et al., 2009; Arkley et al., 2014). Stimulation of the vibrissal primary motor cortex (vM1) has been found to evoke vibrissa movement (Donoghue and Wise, 1982), and vM1 neurons modulate whisking parameters such as frequency and amplitude (Hill et al., 2011; Gerdjikov et al., 2013). Cortical motor commands are considered to play an important role in whisking behavior (Petersen, 2014). The whisking central pattern generator (CPG) in the brainstem controls the facial nuclei (FN) (Moore et al., 2013; Takatoh et al., 2013), which directly drive vibrissa movement (Herfst and Brecht, 2008). The CPG receives cortical input from layer 5 of the vM1 (Alloway et al., 2010; Petersen, 2014). Layer 5 pyramidal neurons of the vM1 are known to include two morphological groups, intratelencephalic (IT) neurons and pyramidal tract (PT) neurons (Shepherd, 2013; Harris and Shepherd, 2015; Kawaguchi, 2017). IT neurons project axons bilaterally only within the telencephalon (mainly the cerebral cortex and striatum) (Veinante and Deschênes, 2003; Alloway et al., 2009), and PT neurons send axon collaterals ipsilaterally to the cerebral cortex and to subcortical structures on the way to the brainstem or spinal cord (Deschênes et al., 1994; Alloway et al., 2008; Kress et al., 2013). In the vibrissa system, these architectures imply that PT neurons provide motor commands mainly for the

ipsilateral cerebral cortex and subcortical structures while IT neurons send motor information only to the bilateral telencephalon. Thus, motor commands conveyed by PT neurons appear to be different from motor-associated information encoded by IT neurons.

Here, we investigated correlations between axonal projection patterns of layer 5 neurons in the vM1 and neuronal firing properties associated with vibrissa movement. Such correlations may reveal how corticofugal circuits contribute to vibrissal motor control and provide a platform for the integration of vibrissa motor information with other signals, such as sensory inputs.

Materials and Methods

Experimental design

We used male Long-Evans rats (weighing 250–350 g) for studies involving intracortical microstimulation ($n = 6$), electrophysiology and anatomy ($n = 40$). Approximately 95 coronal brain slices and 220 sagittal slices per animal were obtained in the anatomical study. All procedures were conducted in accordance with the animal care guidelines recommended by the Institute of Laboratory Animals, Graduate School of Medicine, Kyoto University (approved number: MedKyo16573). All efforts were made to minimize the suffering and number of animals used in this study.

Intracortical microstimulation study

The 3 rats were anesthetized via an intraperitoneal injection of chloral hydrate (35 mg/100 g body weight), and the other 3 rats were under ketamine (75 mg/kg, xylazine, 5 mg/kg) anesthesia. They were fixed in place in a stereotaxic instrument. A craniotomy was performed over the frontal cortex. A single 250- μm diameter parylene-coated tungsten electrode with an impedance of 2 Mohm (A-M systems) was successively lowered at a depth 1,500 μm below the pia surface to stimulate various locations within the cortex. We used twomicrostimulation paradigms to locate areas that led to vibrissal motion. The bipolar current pulses (cathodal first) were delivered at 60 Hz with a duration of 200 μs (20–100 μA) (Haiss and Schwarz, 2005). The monophasic cathodal pulses of 100 μA with a duration of 200 μs each were delivered thorough the microelectrode at 2 ms intervals (Donoghue and Wise, 1982). Visual inspection under a microscope confirmed that the vibrissae moved in response to stimulation.

Surgery

Rats were briefly handled. After the rats were anesthetized via an intraperitoneal injection of chloral hydrate (35 mg/100 g body weight), a lightweight head attachment (Narishige Co.) was surgically attached to the skull, and a reference electrode was implanted in the occipital bone. Two small portions of the left side of the skull were removed: one was located 1.5 mm anterior and 0.75 mm lateral from bregma, and the other was located 2.5 mm anterior and 1.5 mm lateral from bregma (Kleinfeld et al., 2002; Haiss and Schwarz, 2005). Those areas corresponded to the left hemisphere vM1 (Fig. 1). We trimmed all vibrissae on the right side, except the second vibrissa in row C (C2). Retrimming occurred every third day.

Videography

We monitored the position of the right C2 vibrissa in the head-fixed rats using a high-speed camera (CV-035M, Keyence) at 200 Hz (Fig. 2A). Planar images (512 \times 480 pixel) were acquired at a spatial resolution of 100 μm with an infrared light-emitting diode (850 nm) backlight. An image sensor (CV-5500,

Keyence) received data from the high-speed camera and calculated the angle (θ) formed between the anterior-posterior axis of the rat and the center of the vibrissa. We acquired vibrissa movement as the angle $\theta(t)$, where t was the discrete time, on a computer. The time delay (21.8ms), which was caused by the image processing, was compensated in the data analysis.

Behavioral training

After recovering from surgery, the rats were deprived of drinking water in their home cages. The rats were trained to perform a voluntary whisking task for 2 h in an operant system (O'hara & Co.). Training sessions were scheduled two times per day for 5 days. We used a personal computer (Dell) with LabVIEW software (National Instruments) to control the training apparatuses. The rats were monitored using an infrared camera. A 10 ms 6 kHz tone indicated the start of each trial. If a rat continued moving its vibrissae with a frequency greater than 3 Hz and amplitude greater than 3 degrees for 1 s, he received a drop of water from a spout connected to a syringe pump. The intervals between trials ranged from 3,000–4,000 ms.

Decomposition of vibrissa movement

To minimize errors associate with videography, the angle (θ) was corrected to an averaged angle. The averaged angle was the arithmetic mean of the three middle of nine continuous values of the angle occurring from $\theta(t-4)$ to $\theta(t+4)$. We obtained the high-frequency components of the time series of the averaged angle by setting the coefficients of the levels of decomposition corresponding to ≥ 64 samples in the biorthogonal B-spline wavelet transform of order (3, 9) to zero. We acquired the amplitude signal $\theta_{amp}(t)$ from the absolute values of the high-frequency component using the Hilbert transform (Fig. 2B).

Electrophysiological recording and electroporation

We inserted either the palmitoylation site-attached green fluorescent protein (palGFP) (Furuta et al., 2001) sequence or the monomeric red fluorescent protein (pal-mRFP) (Nishino et al., 2008) sequence into the EcoRI/NotI sites of pCAG-EN (Addgene plasmid 11160), resulting in pCAG-palGFP or pCAG-pal-mRFP. The glass electrode (tip resistance, 8 Mohm; tip diameter, 1 μm) was filled with a standard internal solution (140 mM K-gluconate, 5mM KCL, 1mM MgCl_2 , 2mM EGTA, 5mM HEPES, 2mM MgATP; pH 7.2) and 500 ng/ μL plasmid, along with pCAG-palGFP or pCAG-pal-mRFP. The electrode was attached to a pipette holder (MEH2SW, World Precision Instruments) and a fine micromanipulator (DMA-1511, Narishige Co.) on a stereotaxic frame (SR-8N-S, Narishige Co.) and was lowered vertically to record layer 5 pyramidal cells (depth: 1,000–2,000 μm below the pia) in the two areas of the left vM1 where the skull had already been removed. Extracellular signals were amplified (IR-283, Cygnus Tech), band-pass filtered (100 Hz to 2 kHz, 440 instrumentation amplifier, Brownlee Precision), sampled at 10 kHz, and stored on a hard disk for off-line analysis. After completing electrophysiological recording, some recorded neurons (one to two neurons in an animal) received plasmid electroporation. The electrode was disconnected from the amplifier and connected to a stimulus isolator (SS-202J and SEN-301, Nihon Kohden). We applied a cathodal voltage pulse train (–10V, 50 pulses at 50 Hz) to inject the plasmid into the recorded cell (Oyama et al., 2013). The plasmid injections were performed with enough distances (500 μm anterior-posterior coordinate, 1000 μm lateral-medial coordinate) between places of the injections. This enabled us to identify each individual labeled neuron in the tissue sections and associate them with the appropriate electrophysiological records.

Fixation of the brain

The rats were sacrificed 10 days after the plasmid injection. The rats were anesthetized with chloral hydrate (70 mg/100 g) and perfused transcardially with 200 mL of 5 mM sodium phosphate-buffered 0.9% saline (PBS; pH 7.4), followed by 200 mL of 3.7% (w/v) formaldehyde in 0.1 M sodium phosphate buffer (PB; pH 7.4). The brains were removed and postfixed for 2 h at room temperature with the same fixative. After the brains were cryoprotected with 30% (w/v) sucrose in PBS at room temperature overnight, the front portions of the brains (from the frontal pole of the cerebrum to 0.96 mm posterior to bregma) were sliced into 60- μ m-thick coronal sections and the rear portions (from 0.96 mm posterior to bregma to the brainstem) were sliced into 60- μ m-thick sagittal sections using a freezing microtome. Locations were determined using a stereotaxic atlas (Paxinos and Watson, 2007). Sections were serially collected in PB.

Histological staining

All sections were incubated overnight with 0.3 μ g/mL affinity-purified rabbit anti-GFP antibody (Nakamura et al., 2008) or 0.15 μ g/mL affinity-purified rabbit anti-mRFP antibody (Hioki et al., 2010) in PBS containing 0.3% Triton X-100, 0.12% lambda-carrageenan, 0.02% sodium azide, and 1% donkey serum (PBS-XCD). After a rinse with PBS containing 0.3% Triton X-100 (PBS-X), the sections were incubated for 1 h with 10 μ g/mL biotinylated goat anti-rabbit IgG antibody (BA-1000; Vector, Burlingame, CA) and then for 1 h with avidin-biotinylated peroxidase complex (ABC; 1:100; Elite variety, Vector) in PBS-X. After a rinse in 0.1 M PB, we applied the biotinylated tyramine (BT)-glucose oxidase (GO) amplification method (Furuta et al., 2009) to the sagittal sections. The sagittal sections were incubated for 30 min in the BT-GO reaction mixture containing 1.37 μ M BT, 3 μ g/mL of GO (273 U/mg; Nacalai Tesque), 2 mg/mL beta-D-glucose, and 1% BSA in 0.1 M PB, followed by a wash with PBS-X. Subsequently, the sagittal sections were again incubated for 1 h with ABC-Elite in PBS-X. The peroxidase in all sections was visualized using 0.025% diaminobenzidine-4HCl (DAB; Dojindo), 0.625% nickel, and 0.00015% H₂O₂ in 50 mM Tris-HCl (pH 7.6). All incubations were performed at room temperature. All stained sections were serially mounted onto gelatin-coated glass slides and dried overnight. The sections were cleared in ethanol and xylene, and then coverslipped with organic mounting medium MX (Matsunami; Kishiwada, Japan). After reconstruction of palGFP- or pal-mRFP-labeled neurons, the sections were counterstained for Nissl with 1% neutral red to identify cytoarchitecture. The cytoarchitecture was determined based on a stereotaxic atlas (Zilles, 1985; Paxinos and Watson, 2007) and previous reports (Zilles et al., 1980; Kubota et al., 2007; Smith and Alloway, 2013).

Reconstruction and morphological analysis of single vM1 neurons

Whole coronal or sagittal sections were automatically captured as large color images using a TOCO digital slide scanner (CLARO) with a $\times 10$ objective lens (EC Plan-Neofluar; Zeiss; numerical aperture [NA] = 0.30). The obtained images had a spatial resolution of 1.038 \times 1.038 μ m, and the axon fibers were traced and digitized using Canvas 12 software (ACD System International Inc.). We reconstructed the axon fibers as a collection in a two-dimensional plane using computer software (Ohno et al., 2012). Axon density in each targeted brain area was semi-quantitatively evaluated (Table 1 and Table 2). The cell body and dendrites were three-dimensionally reconstructed using Neurolucida computer-assisted neuron tracing system 11 (MBF Bioscience; Williston, VT, USA). The reconstructed dendrites were quantitatively analyzed via Sholl analysis (Sholl, 1953) with Neurolucida-associated software NeuroExplorer (MBF). Data were analyzed per

25 μm concentric circles.

Statistics

We performed statistical analyses using the MATLAB Statistics toolbox. We used an *F-test* to compare the distribution of the LA index of the recorded neurons ($n = 203$) with that of the shuffled data. We compared the LA indexes of the analyzed PT neurons and those of the IT neurons using the Wilcoxon rank-sum test. We also used the Wilcoxon rank-sum test to compare the number of dendritic intersections in the PT and IT neurons. The significance level was set at $p < 0.05$. Group data were expressed as mean \pm SD.

Results

Although previous studies have reported that intracortical microstimulation of the anterior and medial areas of the primary motor cortex (M1) evoke vibrissa movement, the exact location of the vM1 is controversial (Donoghue and Wise, 1982; Kleinfeld et al., 2002; Haiss and Schwarz, 2005). We used bipolar and monophasic stimulation procedures (see Methods) and observed vibrissa movement evoked by microstimulation. Because the penetrations of the electrical recordings in the present study were located within the area where vibrissa movement was elicited by microstimulation (Fig. 1), the recorded neurons was considered to be included in the vM1. Our data indicated that the vM1 area straddled the cingulate cortex (Cg) and the medial and lateral agranular cortices (AGm and AGl) in agreement with the cortical maps of vibrissal movement of previous studies (Kleinfeld et al., 2002; Haiss and Schwarz, 2005). All the neurons described below were recorded in layer 5 of the vM1.

Correlation between whisk amplitude and firing probability of vM1 neurons

A previous study reported that most vM1 neurons encode the amplitude of reciprocal vibrissa movement (Hill et al., 2011). In the present study, to examine the firing properties of vM1 neurons associated with whisk amplitude, we simultaneously recorded neuronal activity in the vM1 and vibrissa movement in head-fixed awake rats (Fig. 2A). Because whisking consists of rhythmic swinging along a longitudinal axis, we analyzed vibrissa movement by digitizing the vibrissal position as the azimuthal angle of the vibrissal shaft in horizontal plane images (Fee et al., 1997). Based on time-dependent changes in the vibrissal angle, we extracted the whisk amplitude using the wavelet transform and the Hilbert transform (Fig. 2B). We compared the distribution of the whisk amplitude during instances of neuronal firing (A_S) with that throughout the total recording (A) for each vM1 neuron (Fig. 2C-G). In some neurons, the distribution of A_S was biased toward a larger amplitude compared with that of A . These neurons were considered to fire preferentially during large-amplitude whisking (Fig. 3A). In contrast, other neurons increased firing when the whisking amplitude was small (Fig. 3B). To quantitatively evaluate the probability of neuronal firing that was correlated with whisk amplitude, we computed the large-amplitude index (LA index) as a measure of the preference for large-whisk amplitude in each neuron (Fig. 2G). The LA index was defined as $P(A_S > A')$, where A' is the median of A . The LA index ranged from 0, when the neuron fired only in a quiet state or during the whisk amplitudes that were smaller than the median, to 1, when the neuron fired only during the whisk amplitudes that were larger than the median.

To assess the distribution of the LA index, we compared the LA indexes of the recorded neurons with

those of shuffled data (control data). The shuffled data was generated by randomly changing the interspike intervals of the recorded neurons while keeping the total numbers of spikes. The distribution of the LA index of all the recorded vM1 neurons ($n = 203$) and shuffled data are shown in [Fig. 3C](#) and [D](#), respectively. Compared with the shuffled data, the LA indexes for recorded vM1 neurons showed significantly wider distribution ($p < 0.001$ by F -test). Dashed lines in [Fig.3C](#) and [D](#) indicate the range of mean ± 2 SD which was calculated from the shuffled data. These contained neurons that tended to fire when the rats made large vibrissa movements (e.g., neuron #073) ([Fig. 3A](#)) and neurons that were active during small-amplitude whisking as well as when the rats were in a quiet state (e.g., neuron #166) ([Fig. 3B](#)). The LA index is thought to be closely related to corticofugal motor commands rather than to sensory information. Specifically, a previous study found a correlation between neuronal activity in the vM1 and whisk amplitude even after deprivation of the infraorbital nerve (Hill et al., 2011).

LA index of PT and IT neurons

After completing the electrophysiological recordings, we injected plasmid, which expresses membrane-targeted fluorescent proteins, into the recorded neurons using the single-cell electroporation technique ([Fig. 2A](#)) (Oyama et al., 2013). After tracing axonal projections from layer 5 of the vM1 at the single-neuron level, we obtained ten neurons (five PT and five IT neurons) that were acceptable for morphological analysis ([Fig. 1](#) and [Fig. 4](#)). Most of the morphologically analyzed neurons (8 neurons) were found single in each brain, while only one brain contained 2 nicely labeled neurons. This is because the success rate of the electroporation in the present study was not so high. In the brain which contained the 2 labeled neurons, the axons derived from the 2 neurons did not overlap each other and thus we could segregate individual axons. The LA indexes of these ten neurons are shown in [Table 1](#) and [Table 2](#). The average of the LA indexes of the five PT neurons was 0.5903, and that of the LA indexes of the five IT neurons was 0.4183. When we sorted the analyzed neurons according to their LA indexes, we found that PT neurons exhibited larger indexes compared with IT neurons ($p = 0.0472$, Wilcoxon rank-sum test) ([Table 1](#) and [Table 2](#)). The mean firing rate of the PT neurons was 9.817 Hz and that of the IT neurons was 3.539 Hz. The difference in firing rates between the PT neurons and the IT neurons was not statistically significant ($p = 0.0732$, paired Student's t -test). Additionally, we did not find significant difference between PT neurons and IT neurons in firing properties associated with other motor variables such as midpoint of whisking, whisk frequency, and duration of protraction and retraction. Our results indicate that long corticofugal circuits to the brainstem were active during large-amplitude whisking. In contrast, corticocallosal neurons were active when the whisking amplitude was small or the vibrissae were at rest. Next, to explore the brain structures where the vM1 neurons sent motor information with respect to the LA index, we examined the axonal morphology of the recorded neurons.

Axonal arborization of PT neurons

The PT neurons labeled in this study sent axon collaterals to the cerebral cortex, striatum, diencephalon, midbrain, pons, and medulla oblongata on the ipsilateral side of their cell bodies before their main axons terminated in the medulla oblongata or spinal cord, and some of their axon collaterals innervated the contralateral lower brainstem ([Table 1](#) and [Table 2](#)). A representative PT neuron (#179) sent its main axon to the spinal cord, and collateral branches to the cerebral cortex (the AGm and forelimb area), caudate putamen ([Fig. 5A](#) and [B](#)), diencephalon (the posterior thalamic nucleus, subthalamic nucleus, and zona

incerta), midbrain (the anterior pretectal nucleus, superior colliculus, and periaqueductal gray), pons (the pontine nuclei and pontine reticular nuclei), and medulla oblongata (the gigantocellular reticular nucleus, medial vestibular nucleus, and intermediate reticular nucleus) on the ipsilateral side of the cell body (Fig. 5B). Axon fibers that innervated the ipsilateral lower brainstem successively reached the pons (the caudal part of the pontine reticular nucleus) and the medulla oblongata (the gigantocellular reticular nucleus, medial vestibular nucleus, and intermediate reticular nucleus) on the contralateral side (Fig. 5B). In the cerebral cortex, most of the examined PT neurons (3 of 5 neurons) expanded axons into the motor cortices adjacent to the cortex where the cell body existed (Fig. 6A), and two PT neurons sent axons to the ipsilateral forelimb area (FL) (Fig. 6B). None of the PT neurons projected to the barrel field of the primary somatosensory cortex (S1BF). In the striatum and diencephalon, PT neurons very often projected ipsilaterally to the caudate putamen (CPu) (5/5), posterior thalamic nucleus (POm) (3/5), subthalamic nucleus (STN) (5/5), and zona incerta (ZI) (5/5) (Fig. 6C and D). Axon collaterals, which were derived from main axons in the internal capsule, entered the thalamus from the rostral side, and innervated the thalamic nuclei. Other collateral branches, which main axons emitted in the caudal side of the internal capsule and cerebral peduncle, reached the STN, ZI, and midbrain structures such as the anterior pretectal nucleus (APT), superior colliculus (SC), and periaqueductal gray/mesencephalic reticular formation.

All five of the examined PT neurons sent axon collaterals to the ipsilateral brainstem, and some of them successively reached contralateral brainstem structures (Table 1 and Table 2). The majority of the PT neurons projected ipsilaterally to the APT (4/5) (Fig. 6E), deep layers of the SC (5/5) (Fig. 6F), and periaqueductal gray/mesencephalic reticular formation (5/5) (Fig. 6G), and one neuron also projected to the contralateral midbrain. Axon collaterals, which were derived from main axons in the longitudinal fasciculus of the pons, always projected to the ipsilateral pontine nuclei (PN) (5/5) (Fig. 6H), and most of the collaterals successively innervated the contralateral PN (3/5). Axon collaterals of three PT neurons innervated the ipsilateral pontine reticular nucleus (Fig. 6I), and two of the three neurons reached the contralateral pontine reticular nucleus. PT neurons sent axon collaterals ipsilaterally to the gigantocellular reticular nucleus (4/5) (Fig. 6J), inferior olive (IO) (2/5) (Fig. 6K), and intermediate reticular nucleus (1/5), and almost half of them also contralaterally innervated the gigantocellular reticular nucleus (2/4), IO (1/2), and intermediate reticular nucleus (1/1).

Three PT neurons (#179, #203, and #098) sent main axons to the pyramidal decussation or the dorsal corticospinal tract, while the main axons of the other two neurons (#168 and #091) terminated in the medullary pyramidal tract. Since the PT neurons sent axon collaterals to brain structures prior to axon termination in the lower brainstem or spinal cord, these structures may share the same vibrissal motor information.

Axonal arborization of IT neurons

A representative IT neuron (#148) sent axons ipsilaterally to the AGm, AGI, S1BF, and CPu, and contralaterally to the AGm, AGI, and CPu through the corpus callosum (Fig. 7). The majority of the IT neurons (4 of 5 neurons) sent axons contralaterally through the corpus callosum to cerebral cortices (Fig. 8A-D) containing the cortical area symmetrical to the location of their cell bodies (Table 1 and Table 2). In two of the five IT neurons, collateral axons were emitted to the ipsilateral FL and S1BF (Fig. 8E and F). Axons of vM1 neurons, which project to these areas, are known to mostly innervate layer 1 and layers 5–6 (Veinante and Deschênes, 2003). In this study, axon fibers were projected to layer 1 and layers 5–6 of the

S1BF (Fig. 8F), and to layers 5–6 of the FL. To summarize with respect to the cortical areas involved, IT neurons projected to the motor cortices related to vM1, FL, and S1BF. Three IT neurons projected to the ipsilateral CPu, and all of the IT neurons sent axons to the contralateral CPu (Fig. 8G and H). None of the IT neurons sent axons to any subcortical areas except the CPu.

Dendritic morphology of PT and IT neurons

Fig. 9A shows the reconstructed somatodendritic morphology of the labeled neurons in this study. Sholl analysis indicated that PT and IT neurons had different numbers of dendritic intersections in distances of 50, 200, and 675–975 μm from the cell bodies ($p = 0.0476$ at 50 μm , $p = 0.0397$ at 200 μm , $p = 0.0317$ at 675 μm , $p = 0.0079$ at 700 μm , $p = 0.0079$ at 725 μm , $p = 0.0079$ at 750 μm , $p = 0.0079$ at 775 μm , $p = 0.0159$ at 800 μm , $p = 0.0159$ at 825 μm , $p = 0.0079$ at 850 μm , $p = 0.0079$ at 875 μm , $p = 0.0079$ at 900 μm , $p = 0.0079$ at 925 μm , $p = 0.0079$ at 950 μm , $p = 0.0476$ at 975 μm , Wilcoxon rank-sum test) (Fig. 9B). The difference in the number of intersections in a distance of 675–975 μm from the cell bodies is likely attributable to the richer apical tuft of PT neurons (Fig. 9A). PT neurons in layer 5 of the motor cortex are known to have longer apical dendrites and prominent terminal arbors in layer 1, and apical dendrites of IT neurons terminate in the middle layers (Veinante and Deschênes, 2003; Kim et al., 2015). Therefore, our result was in agreement with previous reports. The rostromedial portion of the ventral anterior-ventral lateral motor thalamic nuclei (VA-VL) projects to layer 1 of the motor cortex, and the caudolateral portion of the VA-VL innervates the middle layers of the motor cortex (Kuramoto et al., 2009). The basal ganglia send GABAergic efferent projections to the rostromedial portion of the VA-VL, while glutamatergic input from the cerebellum enters the caudolateral portion (Kuramoto et al., 2009). Dendritic morphology indicated that the information from the basal ganglia may be sent not to IT neurons but to PT neurons. The differences in firing properties between PT and IT neurons are thought to relate to differences in their dendritic inputs.

Discussion

In the present study, we demonstrated that PT neurons in layer 5 of the vM1 preferentially fired when rats made large-amplitude whisking, while IT neurons showed high activity during small or null whisking. Furthermore, we described detailed projection patterns of descending axons derived from these two groups of layer 5 neurons at the individual neuron level. We used the single neuron labeling technique combined with the simultaneous recording of vibrissal movement and single neuron firing in awake rats to demonstrate, for the first time, a direct correspondence between firing property and morphological classification in layer 5 neurons in the cortex according to axonal distribution (Shepherd, 2013; Harris and Shepherd, 2015). If the two different corticofugal circuits derived from the motor cortex encode motor information differently, the present findings provide a basis for understanding of mechanisms of motor control and motor-associated information processing. In the previous studies where they analyzed correlations between firing properties of neurons and anatomical data such as location of cell bodies or mRNA expressions (Isomura et al., 2009; Deschenes et al., 2016), juxtacellular recording and labeling technique that enables researchers to visualize morphology of single neurons electrophysiologically identified by unit recordings (Pinault, 1996) was used. On the other hand, it is actually difficult to clearly label long projecting axons by the conventional juxtacellular labeling technique, because dye injected into a cell body is considered to be delivered to axons by diffusion and the concentration of the dye in the distal part of the axons is low. The gene transfer of plasmids

encoding fluorescent proteins by the single-neuron electroporation increase labeling intensity and thus enable the more precise analysis of the axonal arborization at a single-neuron level.

Some PT neurons have been found to send axons to the whisking CPG in the lower brainstem (Moore et al., 2013; Takatoh et al., 2013; Kita et al., 2014). The excitatory input from PT neurons has the potential to activate the FN through the CPG when the whisking amplitude is large. Our results suggest that the principal role of PT neurons is to induce large-amplitude whisking through the CPG and FN. PT neurons sent axons not only to the CPG but also to many other subcortical regions. The pons and medulla oblongata received abundant axon collaterals from long descending PT neuron projections, and most PT neurons projected to the PN and IO. Since these nuclei relay information to the cerebellum, copies of motor commands are expected to influence cerebellar functions, such as the coordination, precision, and accurate timing of movements (Wolf et al., 2009). In addition, all of the PT neurons in our study projected ipsilaterally not only to the CPu but also to the STN and ZI. These regions are known to have strong connections with the basal ganglia (Kita et al., 2014), which is associated with voluntary motor movement, learning, cognition, and emotion (Stocco et al., 2010). As previously reported (Deschênes et al., 1994; Alloway et al., 2009; Kita and Kita, 2012), most of the five PT neurons also sent axons to the POm, APT, and SC. The APT and ZI are known to innervate the POm, and have a strong inhibitory influence on the thalamus (Giber et al., 2008). The SC has many functions including control of vibrissa movement (Hemelt and Keller, 2008), vibrissal sensory processing (Bezdudnaya and Castro-Alamancos, 2014), and locomotion (Felsen and Mainen, 2008). Whisking motor commands may be integrated with such information in the SC, and thus contribute to exploring activity. Overall, our data and that from previous studies indicate that copies of cortical motor commands given by PT neurons are shared with the cerebellum, basal ganglia, and SC, and that such data contribute to motor-associated functions including fine movement and motor control.

The decrease in IT neuronal firing rate during large-amplitude whisking indicates that the motor information given by IT neurons might differ from the motor commands that directly move the vibrissae. Given that the firing properties and axonal projections of IT neurons are different from those of PT neurons, IT neurons likely possess different roles in motor function.

Gao et al. (2003) reported that unilateral lesion of the motor cortex caused changes of whisking amplitude and velocity not only on the contralateral side but also on the ipsilateral side that is mainly modulated by the contralateral motor cortex (Gao et al., 2003). This suggests that the activity of the contralateral cortex was affected by the elimination of cortico-callosal axons from the lesioned cortex. In awake animals, a neuron group in layer 2/3 of the frontal cortex is known to exert axonal projection to the contralateral cortex (Kawaguchi, 2017) and has been reported to reduce firing rate of the target area during whisking (Sreenivasan et al., 2016). Because one of the most striking characteristics of axonal morphology in IT neurons is the cortico-callosal projection (Fig. 7 and Fig. 8 A–D) (Shepherd, 2013) similarly with the group of layer 2/3 neurons, it is speculated that IT neurons cooperate with the cortico-callosal neurons in layer 2/3 to associate the right and left cortex and to contribute to the coordinated movement of bilateral vibrissae.

The CPu, which is a major component of the basal ganglia (Gerfen, 1992), was an important target for the IT neurons examined in this study. Because most of the IT neurons projected bilaterally to the CPu, IT neurons might affect bilateral basal ganglia activities. Additionally, the present study shows that two IT neurons sent axons to the ipsilateral S1BF, while no PT neurons projected to the S1BF, in agreement with the previous report where most of motor cortex neurons projecting to the S1BF were IT neurons (Veinante and Deschênes, 2003). S1BF neurons are thought to receive not only tactile signals but also other inputs

including those associated with decision making (O'Connor et al., 2010) and vibrissal motor information (Hill et al., 2011). Our results suggest that vibrissal motor information processed by IT neurons is sent directly to S1BF, and thus that this information is used for sensorimotor integration.

References

- Alloway KD, Olson ML, Smith JB (2008) Contralateral corticothalamic projections from M1 whisker cortex: potential route for modulating hemispheric interactions. *J Comp Neurol* 510:100-116.
- Alloway KD, Smith JB, Beauchemin KJ (2010) Quantitative analysis of the bilateral brainstem projections from the whisker and forepaw regions in rat primary motor cortex. *J Comp Neurol* 518:4546-4566.
- Alloway KD, Smith JB, Beauchemin KJ, Olson ML (2009) Bilateral projections from rat M1 whisker cortex to the neostriatum, thalamus, and claustrum: forebrain circuits for modulating whisking behavior. *J Comp Neurol* 515:548-564.
- Arkley K, Grant RA, Mitchinson B, Prescott TJ (2014) Strategy change in vibrissal active sensing during rat locomotion. *Curr Biol* 24:1507-1512.
- Bezdudnaya T, Castro-Alamancos MA (2014) Neuromodulation of whisking related neural activity in superior colliculus. *J Neurosci* 34:7683-7695.
- Deschênes M, Bourassa J, Pinault D (1994) Corticothalamic projections from layer V cells in rat are collaterals of long-range corticofugal axons. *Brain Res* 664:215-219.
- Deschenes M, Takatoh J, Kurnikova A, Moore JD, Demers M, Elbaz M, Furuta T, Wang F, Kleinfeld D (2016) Inhibition, Not Excitation, Drives Rhythmic Whisking. *Neuron* 90:374-387.
- Diamond ME, von Heimendahl M, Knutsen PM, Kleinfeld D, Ahissar E (2008) 'Where' and 'what' in the whisker sensorimotor system. *Nat Rev Neurosci* 9:601-612.
- Donoghue JP, Wise SP (1982) The motor cortex of the rat: cytoarchitecture and microstimulation mapping. *J Comp Neurol* 212:76-88.
- Fee MS, Mitra PP, Kleinfeld D (1997) Central versus peripheral determinants of patterned spike activity in rat vibrissa cortex during whisking. *J Neurophysiol* 78:1144-1149.
- Felsen G, Mainen ZF (2008) Neural substrates of sensory-guided locomotor decisions in the rat superior colliculus. *Neuron* 60:137-148.
- Furuta T, Kaneko T, Deschênes M (2009) Septal neurons in barrel cortex derive their receptive field input from the lemniscal pathway. *J Neurosci* 29:4089-4095.
- Furuta T, Tomioka R, Taki K, Nakamura K, Tamamaki N, Kaneko T (2001) In vivo transduction of central neurons using recombinant sindbis virus: golgi-like labeling of dendrites and axons with membrane-targeted fluorescent proteins. *J Histochem Cytochem* 49:1497-1507.
- Gao P, Hattox AM, Jones LM, Keller A, Zeigler HP (2003) Whisker motor cortex ablation and whisker movement patterns. *Somatosens Mot Res* 20:191-198.
- Gerdjikov TV, Haiss F, Rodriguez-Sierra OE, Schwarz C (2013) Rhythmic whisking area (RW) in rat primary motor cortex: an internal monitor of movement-related signals? *J Neurosci* 33:14193-14204.
- Gerfen CR (1992) The neostriatal mosaic: multiple levels of compartmental organization. *Trends Neurosci* 15:133-139.
- Giber K, Slezia A, Bokor H, Bodor AL, Ludanyi A, Katona I, Acsady L (2008) Heterogeneous output pathways link the anterior pretectal nucleus with the zona incerta and the thalamus in rat. *J Comp*

Neurol 506:122-140.

- Grant RA, Mitchinson B, Fox CW, Prescott TJ (2009) Active touch sensing in the rat: anticipatory and regulatory control of whisker movements during surface exploration. *J Neurophysiol* 101:862-874.
- Haiss F, Schwarz C (2005) Spatial segregation of different modes of movement control in the whisker representation of rat primary motor cortex. *J Neurosci* 25:1579-1587.
- Harris KD, Shepherd GM (2015) The neocortical circuit: themes and variations. *Nat Neurosci* 18:170-181.
- Hemelt ME, Keller A (2008) Superior colliculus control of vibrissa movements. *J Neurophysiol* 100:1245-1254.
- Herfst LJ, Brecht M (2008) Whisker movements evoked by stimulation of single motor neurons in the facial nucleus of the rat. *J Neurophysiol* 99:2821-2832.
- Hill DN, Curtis JC, Moore JD, Kleinfeld D (2011) Primary motor cortex reports efferent control of vibrissa motion on multiple timescales. *Neuron* 72:344-356.
- Hioki H, Nakamura H, Ma YF, Konno M, Hayakawa T, Nakamura KC, Fujiyama F, Kaneko T (2010) Vesicular glutamate transporter 3-expressing nonserotonergic projection neurons constitute a subregion in the rat midbrain raphe nuclei. *J Comp Neurol* 518:668-686.
- Isomura Y, Harukuni R, Takekawa T, Aizawa H, Fukai T (2009) Microcircuitry coordination of cortical motor information in self-initiation of voluntary movements. *Nat Neurosci* 12:1586-1593.
- Kawaguchi Y (2017) Pyramidal Cell Subtypes and Their Synaptic Connections in Layer 5 of Rat Frontal Cortex. *Cereb Cortex* 27:5755-5771.
- Kim EJ, Juavinett AL, Kyubwa EM, Jacobs MW, Callaway EM (2015) Three Types of Cortical Layer 5 Neurons That Differ in Brain-wide Connectivity and Function. *Neuron* 88:1253-1267.
- Kita T, Kita H (2012) The subthalamic nucleus is one of multiple innervation sites for long-range corticofugal axons: a single-axon tracing study in the rat. *J Neurosci* 32:5990-5999.
- Kita T, Osten P, Kita H (2014) Rat subthalamic nucleus and zona incerta share extensively overlapped representations of cortical functional territories. *J Comp Neurol* 522:4043-4056.
- Kleinfeld D, Deschênes M (2011) Neuronal basis for object location in the vibrissa scanning sensorimotor system. *Neuron* 72:455-468.
- Kleinfeld D, Sachdev RNS, Merchant LM, Jarvis MR, Ebner FF (2002) Adaptive filtering of vibrissa input in motor cortex of rat. *Neuron* 34:1021-1034.
- Kress GJ, Yamawaki N, Wokosin DL, Wickersham IR, Shepherd GM, Surmeier DJ (2013) Convergent cortical innervation of striatal projection neurons. *Nat Neurosci* 16:665-667.
- Kubota Y, Hatada S, Kondo S, Karube F, Kawaguchi Y (2007) Neocortical inhibitory terminals innervate dendritic spines targeted by thalamocortical afferents. *J Neurosci* 27:1139-1150.
- Kuramoto E, Furuta T, Nakamura KC, Unzai T, Hioki H, Kaneko T (2009) Two types of thalamocortical projections from the motor thalamic nuclei of the rat: a single neuron-tracing study using viral vectors. *Cereb Cortex* 19:2065-2077.
- Mitchinson B, Martin CJ, Grant RA, Prescott TJ (2007) Feedback control in active sensing: rat exploratory whisking is modulated by environmental contact. *Proc Biol Sci* 274:1035-1041.
- Mitchinson B, Grant RA, Arkley K, Rankov V, Perkon I, Prescott TJ (2011) Active vibrissal sensing in rodents and marsupials. *Philos Trans R Soc Lond B Biol Sci* 366:3037-3048.
- Moore JD, Deschênes M, Furuta T, Huber D, Smear MC, Demers M, Kleinfeld D (2013) Hierarchy of orofacial rhythms revealed through whisking and breathing. *Nature* 497:205-210.

- Nakamura KC, Kameda H, Koshimizu Y, Yanagawa Y, Kaneko T (2008) Production and histological application of affinity-purified antibodies to heat-denatured green fluorescent protein. *J Histochem Cytochem* 56:647-657.
- Nishino E, Yamada R, Kuba H, Hioki H, Furuta T, Kaneko T, Ohmori H (2008) Sound-intensity-dependent compensation for the small interaural time difference cue for sound source localization. *J Neurosci* 28:7153-7164.
- O'Connor DH, Peron SP, Huber D, Svoboda K (2010) Neural activity in barrel cortex underlying vibrissa-based object localization in mice. *Neuron* 67:1048-1061.
- Ohno S, Kuramoto E, Furuta T, Hioki H, Tanaka YR, Fujiyama F, Sonomura T, Uemura M, Sugiyama K, Kaneko T (2012) A morphological analysis of thalamocortical axon fibers of rat posterior thalamic nuclei: a single neuron tracing study with viral vectors. *Cereb Cortex* 22:2840-2857.
- Oyama K, Ohara S, Sato S, Karube F, Fujiyama F, Isomura Y, Mushiake H, Iijima T, Tsutsui K (2013) Long-lasting single-neuron labeling by in vivo electroporation without microscopic guidance. *J Neurosci Methods* 218:139-147.
- Paxinos G, Watson C (2007) *The rat brain in stereotaxic coordinates*, 6th Edition. London: Academic press.
- Petersen CC (2014) Cortical control of whisker movement. *Annu Rev Neurosci* 37:183-203.
- Pinault D (1996) A novel single-cell staining procedure performed in vivo under electrophysiological control: morpho-functional features of juxtacellularly labeled thalamic cells and other central neurons with biocytin or Neurobiotin. *Journal of Neuroscience methods* 65:113-136.
- Shepherd GM (2013) Corticostriatal connectivity and its role in disease. *Nat Rev Neurosci* 14:278-291.
- Sholl DA (1953) Dendritic organization in the neurons of the visual and motor cortices of the cat. *J Anat* 87:387-406.
- Smith JB, Alloway KD (2013) Rat whisker motor cortex is subdivided into sensory-input and motor-output areas. *Front Neural Circuits* 7:4.
- Sreenivasan V, Esmaeili V, Kiritani T, Galan K, Crochet S, Petersen CCH (2016) Movement Initiation Signals in Mouse Whisker Motor Cortex. *Neuron* 92:1368-1382.
- Stocco A, Lebiere C, Anderson JR (2010) Conditional routing of information to the cortex: a model of the basal ganglia's role in cognitive coordination. *Psychol Rev* 117:541-574.
- Takato J, Nelson A, Zhou X, Bolton MM, Ehlers MD, Arenkiel BR, Mooney R, Wang F (2013) New modules are added to vibrissal premotor circuitry with the emergence of exploratory whisking. *Neuron* 77:346-360.
- Towal RB, Hartmann MJ (2006) Right-left asymmetries in the whisking behavior of rats anticipate head movements. *J Neurosci* 26:8838-8846.
- Veinante P, Deschênes M (2003) Single-cell study of motor cortex projections to the barrel field in rats. *J Comp Neurol* 464:98-103.
- Welker WI (1964) Analysis of sniffing of the albino rat. *Behaviour* 22:223-244.
- Wolf U, Rapoport M, Schweizer TA (2009) Evaluating the affective component of the cerebellar cognitive affective syndrome. *J neuropsychiatry Clin neurosci* 21:245-253.
- Zilles K (1985) *The cortex of the rat*. Berlin: Springer Berlin Heidelberg.
- Zilles K, Zilles B, Schleicher A (1980) A quantitative approach to cytoarchitectonics. *Anat Embryol* 159:335-360.

Table 1. Summary of the distribution of labeled axon fibers ipsilateral to the cell body

Neuron number	LA index	Projection type	Cerebral cortex				Striatum		Diencephalon					Midbrain			Pons		Medulla oblongata						
			Cg	AGm	AGl	FL	S1BF	CPu	AV	POm	STN	ZI	Hb	APT	RN	SC	PAG/ mRt	PN	PnC	PnO/	Gi	IO	IRt	MV	
148	0.2409	IT	-	++	+++*	++	++	+++	-	-	-	-	-	-	-	-	-	-	-	-	-	-	-	-	
089	0.3870	IT	+++*	++	++	-	-	-	-	-	-	-	-	-	-	-	-	-	-	-	-	-	-	-	
168	0.4070	PT	-	+++*	-	-	-	+	-	+	+	++	-	+	-	+	++	+++	-	-	-	-	-	-	
129	0.4665	IT	-	+++*	++	-	++	-	-	-	-	-	-	-	-	-	-	-	-	-	-	-	-	-	
118	0.4825	IT	+	+++*	++	-	-	++	-	-	-	-	-	-	-	-	-	-	-	-	-	-	-	-	
119	0.5147	IT	+++*	-	-	-	-	+++	-	-	-	-	-	-	-	-	-	-	-	-	-	-	-	-	
179	0.5149	PT	-	+++	+++*	+	-	+	-	++	+	+++	-	+	-	++	++	+++	++	++	++	+	+	+++	++
203	0.5987	PT	+	+++*	-	-	-	++	-	++	+	++	-	+	-	++	+++	++	-	+	+	-	-	-	
091	0.6875	PT	-	+++*	+	-	-	++	-	-	+	++	-	+	+	+	+++	++	+++	++	+	+	++	++	
098	0.7434	PT	++	+++*	-	+	-	++	+	-	+	++	+	-	-	+	+++	++	++	+	-	-	-	-	

Axon density was semi-quantitatively evaluated and classified according to the following standards: +++, two or more axonal clusters; ++, one cluster; +, no cluster but axon fibers present; -, no axon fibers. * indicates the location of the cell body. The vibrissal primary motor cortex (vM1) was confirmed by intracortical microstimulation. The vM1 area straddled the cingulate cortex (Cg), as well as the medial and lateral agranular cortices (AG).

Abbreviations:

AGl, lateral agranular cortex; AGm, medial agranular cortex; APT, anterior pretectal nucleus; AV, anteroventral thalamic nucleus; CPu, caudate putamen; FL, forelimb area; Gi, gigantocellular reticular nucleus; Hb, habenular nucleus; IO, inferior olive; IRt, intermediate reticular nucleus; LA index; large-amplitude index; MV, medial vestibular nucleus; mRt, mesencephalic reticular formation; PAG, periaqueductal gray; PN, pontine nuclei; PnC, caudal part of pontine reticular nucleus; PnO, oral part of pontine reticular nucleus; POm, posterior thalamic nuclei; RN, red nucleus; SC, superior colliculus; STN, subthalamic nucleus; S1BF, barrel field of primary somatosensory cortex; ZI, zona incerta.

Table 2. Summary of the distribution of labeled axon fibers contralateral to the cell body

Neuron number	LA index	Projection type	Cerebral cortex				Striatum		Diencephalon					Midbrain			Pons		Medulla oblongata					
			Cg	AGm	AGl	FL	S1BF	CPu	AV	POm	STN	ZI	Hb	APT	RN	SC	PAG/ mRt	PN	PnC	PnO/	Gi	IO	IRt	MV
148	0.2409	IT	-	+	++	-	-	+++	-	-	-	-	-	-	-	-	-	-	-	-	-	-	-	-
089	0.3870	IT	++	+	-	-	-	++	-	-	-	-	-	-	-	-	-	-	-	-	-	-	-	-
168	0.4070	PT	-	-	-	-	-	-	-	-	-	-	-	-	-	-	++	-	-	-	-	-	-	-
129	0.4665	IT	-	-	-	-	-	+++	-	-	-	-	-	-	-	-	-	-	-	-	-	-	-	-
118	0.4825	IT	-	+	-	-	-	++	-	-	-	-	-	-	-	-	-	-	-	-	-	-	-	-
119	0.5147	IT	++	-	-	-	-	++	-	-	-	-	-	-	-	-	-	-	-	-	-	-	-	-
179	0.5149	PT	-	-	-	-	-	-	-	-	-	-	-	-	-	-	-	++	+	-	++	++	-	-
203	0.5987	PT	-	-	-	-	-	-	-	-	-	-	-	-	-	-	-	-	-	+	-	-	-	-
091	0.6875	PT	-	-	-	-	-	-	-	-	-	-	-	+	+	+	++	++	+	+	-	++	++	++
098	0.7434	PT	-	-	-	-	-	-	-	-	-	-	-	-	-	-	+	-	-	-	-	-	-	-

Semi-quantitative evaluation of axon density. Criteria and abbreviations are the same as those used in Table 1.

Figure Legends

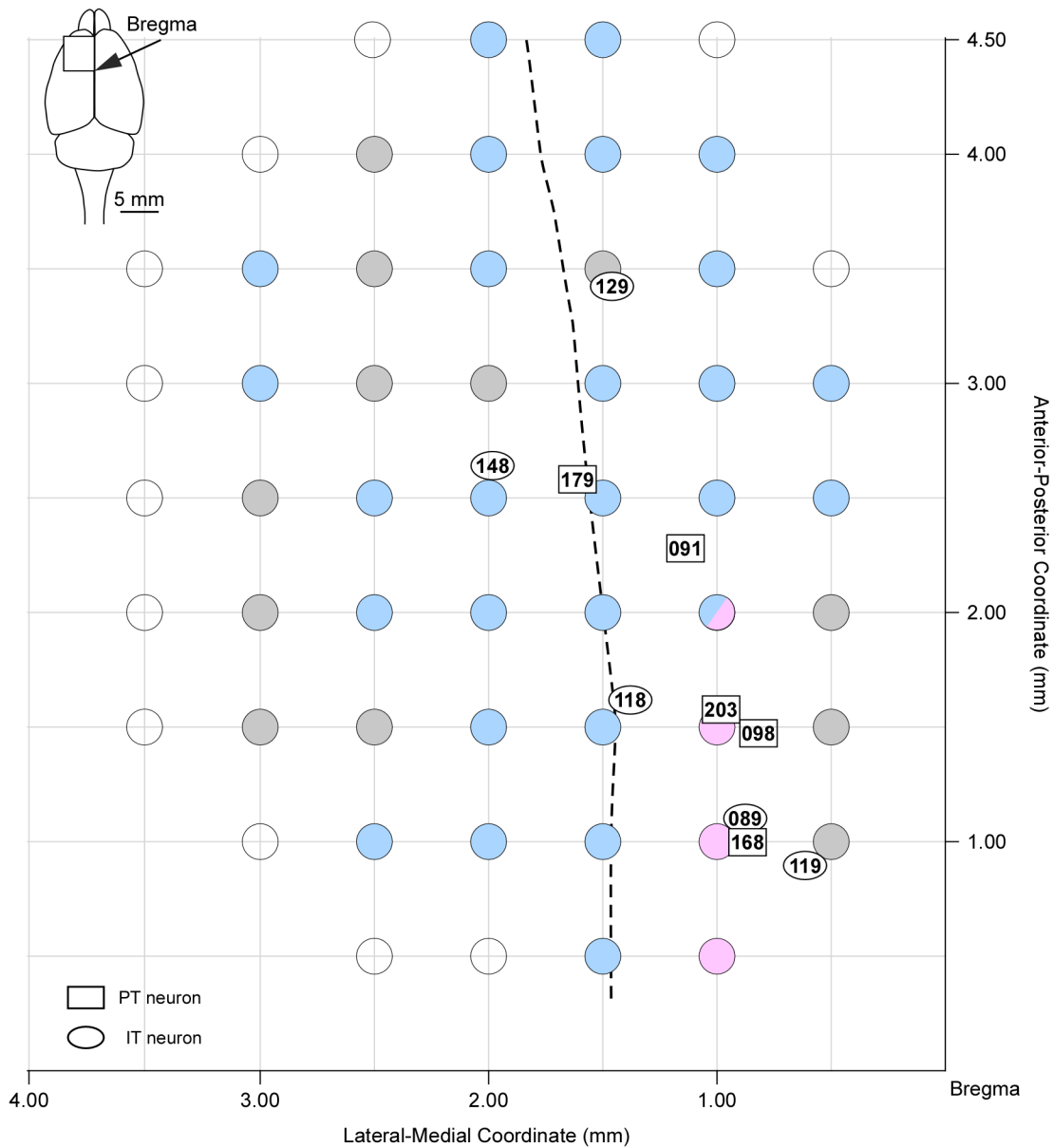


Figure 1. Vibrissa movement map of responses to intracortical microstimulation in the frontal cortex. Microstimulations evoked protractions (magenta filled circles), retractions (cyan filled circles) and vibrations of small amplitudes without any dominance of protraction or retraction (gray filled circles). Microstimulations in a location (2 mm rostral, 1 mm lateral to the bregma) induced both protractions (1 rat) and retractions (2 rats). Open circles indicate places where the microstimulations did not cause any vibrissal movement. Rectangles and ovals indicate the locations of cell bodies of pyramidal tract (PT) and intratelencephalic (IT) neurons, respectively. Numbers within symbols denote the neuron number. Dashed line shows the boundary between the AGm and AGI at a depth of layer 5.

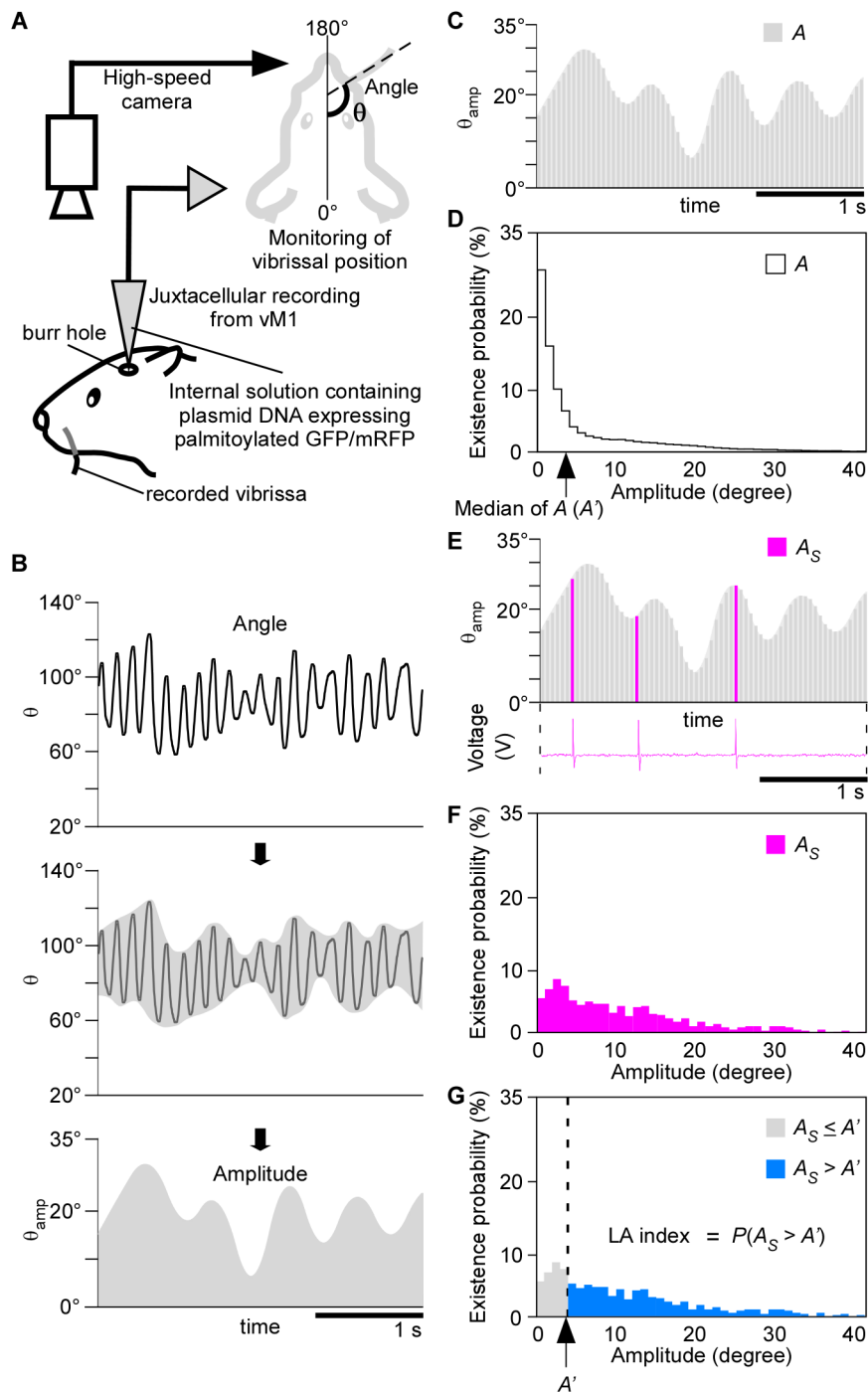


Figure 2. The large-amplitude index (LA index) represents the preference of each unit for large whisking. **A**, Schematic diagram describing vibrissal position monitoring via a high-speed camera and juxtacellular recording from the vibrissal primary motor cortex (vM1) on the side contralateral to the recorded vibrissa. **B**, Whisk amplitude (θ_{amp}) was calculated using the wavelet transform and the Hilbert transform. **C**, We continuously measured whisk amplitude (A) while recording neuronal activity. **D**, Histogram showing the distribution of the existence probabilities of A . The median of A (A') in this neuron was 4° (arrow). **E**, A_S was defined as the whisk amplitude during instances of neuronal spiking. **F**, Histogram showing the distribution of the existence probabilities of A_S . **G**, The LA index was defined as $P(A_S > A)$.

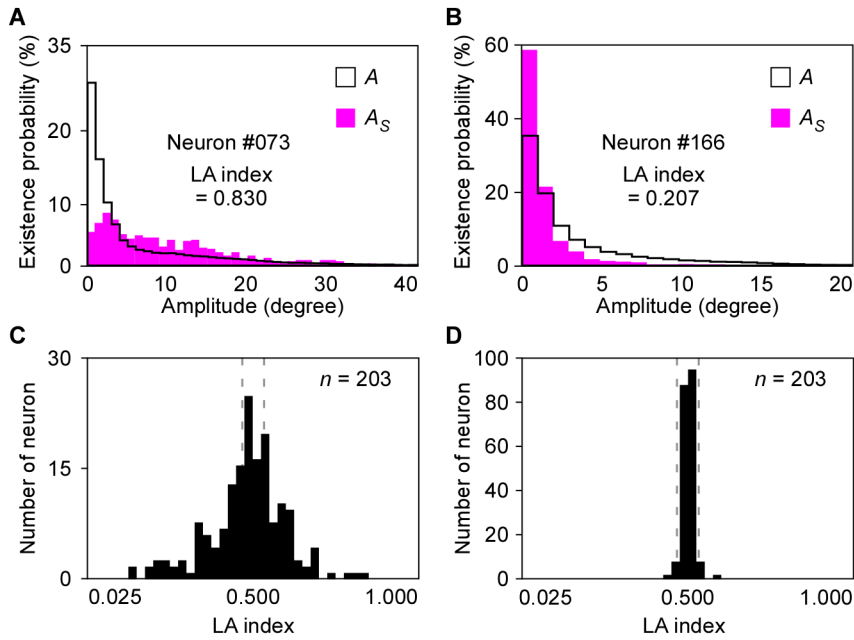


Figure 3. LA indexes of vM1 neurons and the shuffled data. **A**, Representative example of a large LA index. Compared with A , A_S was lower during small-amplitude whisking and higher during large-amplitude whisking in neuron #073. Neuron #073 tended to fire during large-amplitude whisking. **B**, Representative example of a small LA index. **C**, The distribution of LA indexes for all recorded vM1 neurons. **D**, Compared with the shuffled data, the LA indexes for recorded vM1 neurons showed significantly wider distribution ($p < 0.001$, F -test). Dashed lines in **C** and **D** indicate the range of mean \pm 2 SD which was calculated from the shuffled data.

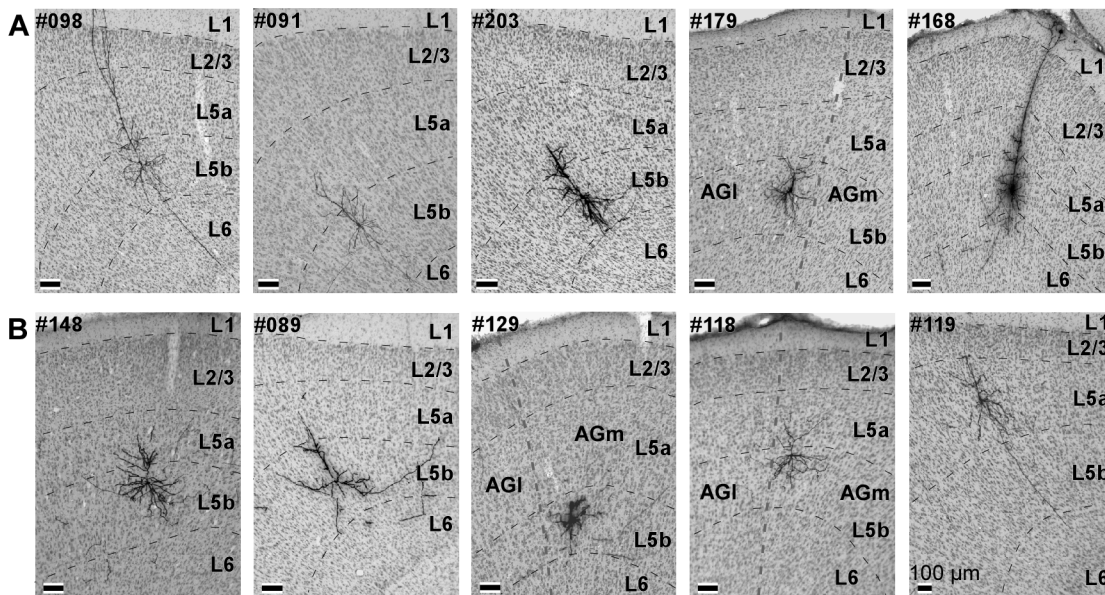


Figure 4. Cell bodies of the ten analyzed neurons. **A**, Cell bodies of the PT neurons were visualized via the immunoperoxidase method. Cortical layers in coronal sections were identified via Nissl staining. All cell bodies of labeled vM1 neurons were localized in layer 5. **B**, Cell bodies of the IT neurons. Thick dashed lines (#179, #129, #118) indicate the boundary between the AGm and AGI.

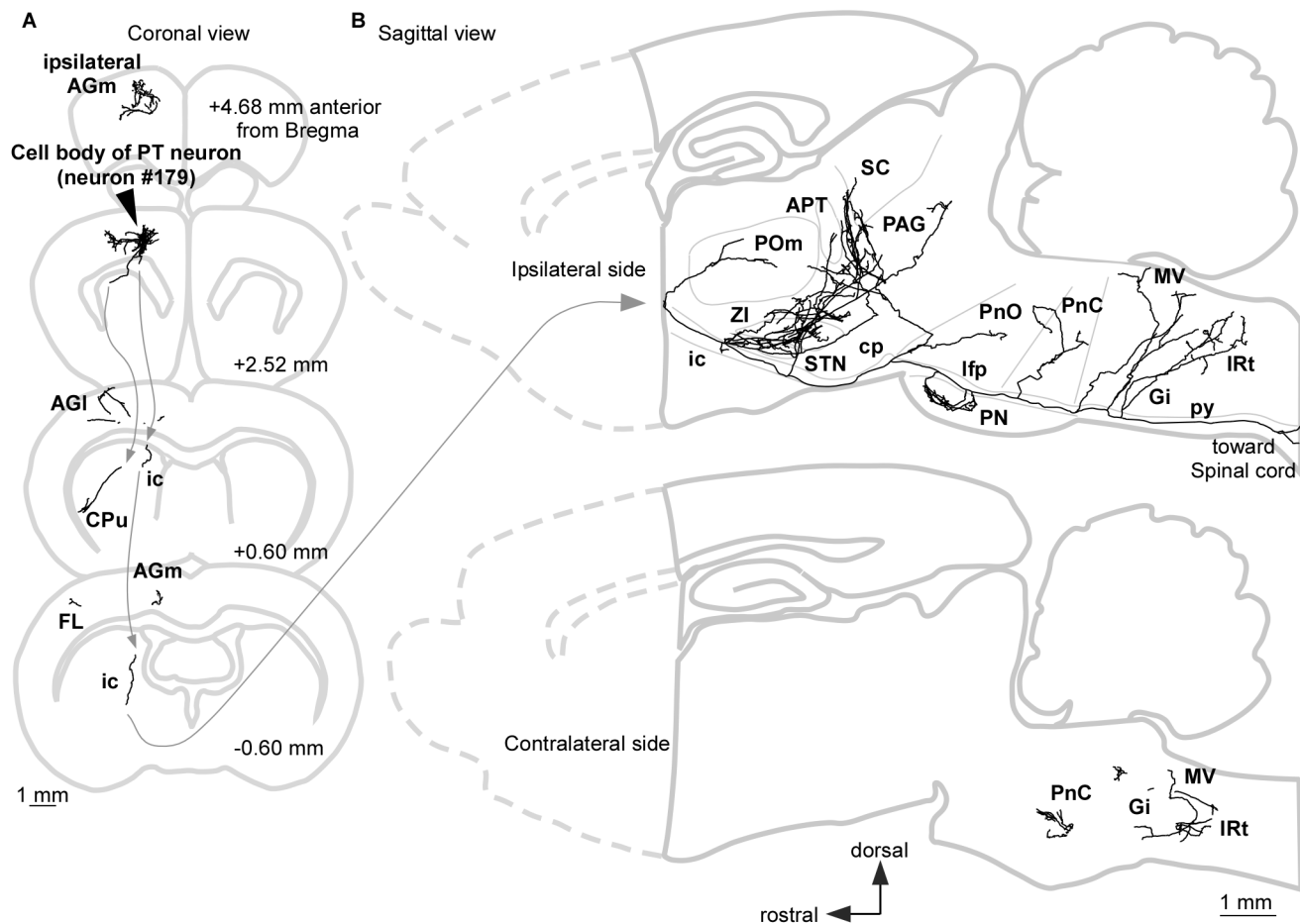


Figure 5. Reconstructed axonal arbor of a representative single PT neuron (#179; LA index was 0.5149), which exhibited a larger LA index than 0.5. **A**, Projected axonal arborization to the coronal planes. This neuron sent its main axon to the spinal cord, and projected axon collaterals to the lateral agranular cortex (AGI), forelimb area (FL), and caudate putamen (CPu) on the ipsilateral side of the cell body. **B**, Projected axonal arborization to the sagittal planes. Upper and lower drawings indicate axonal fibers on the ipsilateral and contralateral sides of the cell body, respectively. This neuron mainly projected to the ipsilateral subcortical areas. Some of the axon collaterals reached the contralateral lower brainstem. AGm, medial agranular cortex; APT, anterior pretectal nucleus; cp, cerebral peduncle; csc, commissure of the superior colliculus; ic, internal capsule; Gi, gigantocellular reticular nucleus; IO, inferior olive; IRt, intermediate reticular nucleus; lfp, longitudinal fasciculus of the pons; MV, medial vestibular nucleus; PAG, periaqueductal gray; PN, pontine nuclei; PnO/PnC, oral part and/or caudal part of the pontine reticular nucleus; POm, posterior thalamic nuclei; py, pyramidal tract; SC, superior colliculus; STN, subthalamic nucleus; ZI, zona incerta.

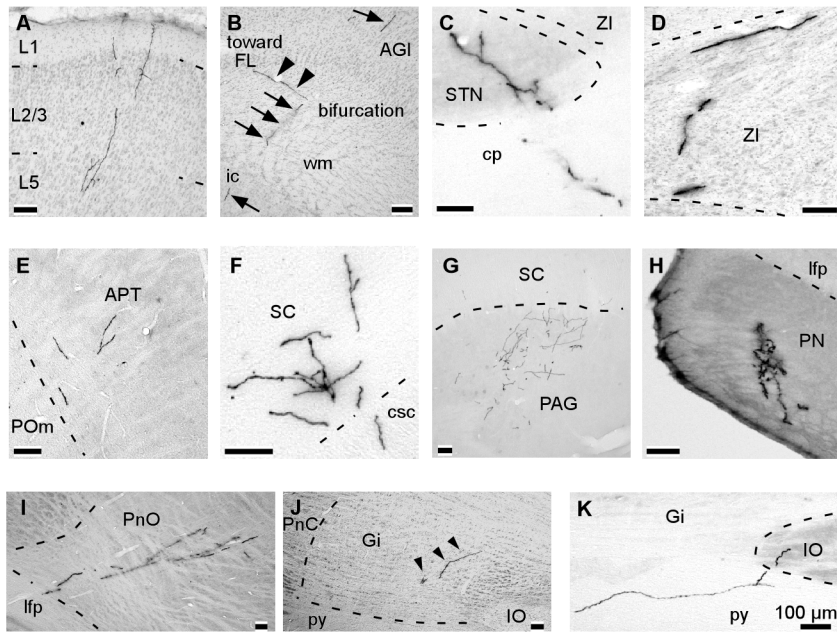


Figure 6. Representative examples of axonal collaterals in the target structures of PT neurons. These photos were obtained from multiple PT neurons. **A**, Axon collaterals in layers 1–5 of the ipsilateral cingulate cortex. **B**, The main axon emitted a branch reaching the FL just before entering the ic. Arrows and arrowheads indicate the main axon and the branch, respectively. **C and D**, All of the PT neurons ipsilaterally projected to the STN and the ZI. **E**, Most PT neurons sent axon collaterals to the APT. **F and G**, all neurons sent axon collaterals to the deep layers of the SC and PAG in the ipsilateral midbrain. **H**, All of the PT neurons sent axon collaterals to the PN. **I and J**, most neurons innervated the ipsilateral PnO and Gi. Arrowheads indicate axonal collaterals. **K**, Two neurons projected to the ipsilateral IO.

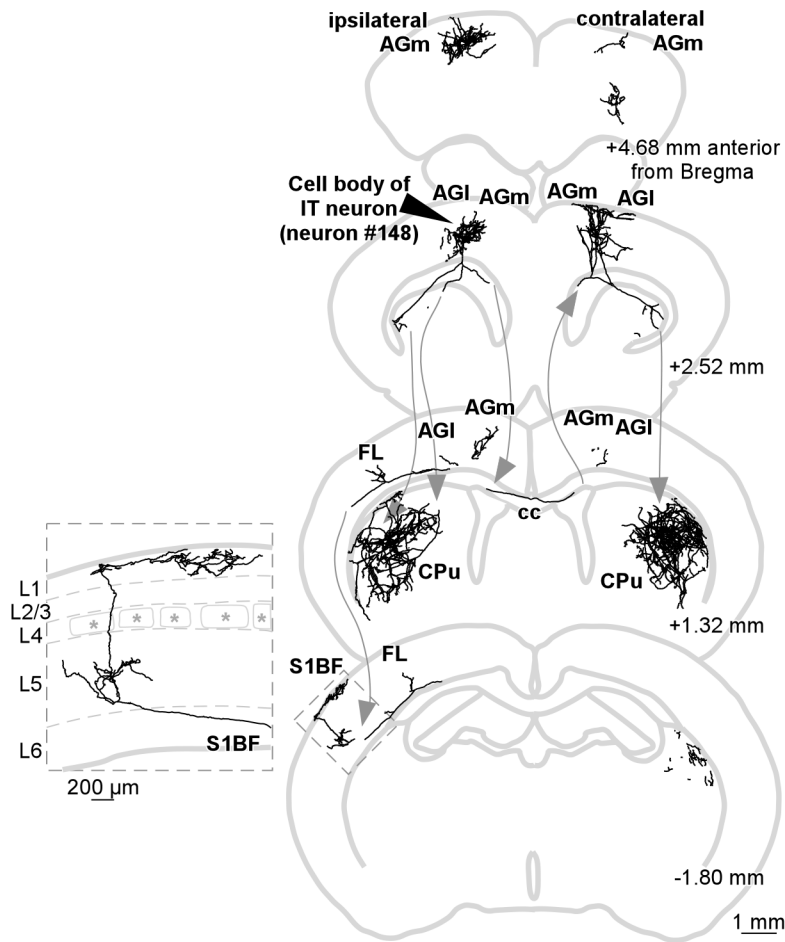


Figure 7. Reconstructed axonal arbor of a single IT neuron (#148; LA index was 0.2409), which exhibited a smaller LA index than 0.5. Axonal arborization of the barrel field of the primary somatosensory cortex (S1BF) (the rectangle) is magnified in the left-hand panel.

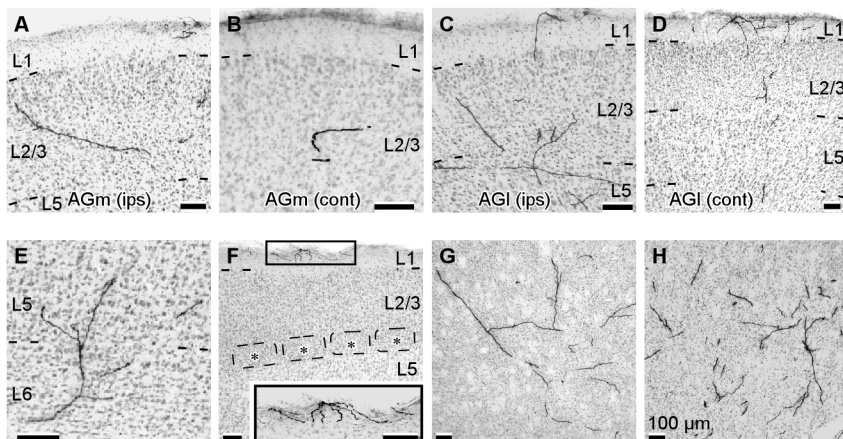


Figure 8. Representative examples of axon collaterals in the target structures of IT neurons. These photos were obtained from multiple IT neurons. **A and B**, axon fibers of IT neurons reached the upper layers (layers 1–2/3) of the ipsilateral AGm and contralateral AGm. **C and D**, IT neurons sent axons to layers 1–5 of the ipsilateral AGI and layers 1–5 of the contralateral AGI. **E**, Axon fibers in layer 5–6 of the ipsilateral FL. **F**, Two of the five IT neurons projected to layers 5–6 and layer 1 of the ipsilateral S1BF. Barrels are indicated by

asterisks. The inset gives a magnified view of the rectangular area. **G**, Three of the five IT neurons projected to the ipsilateral CPU. **H**, All of the IT neurons innervated the contralateral CPU.

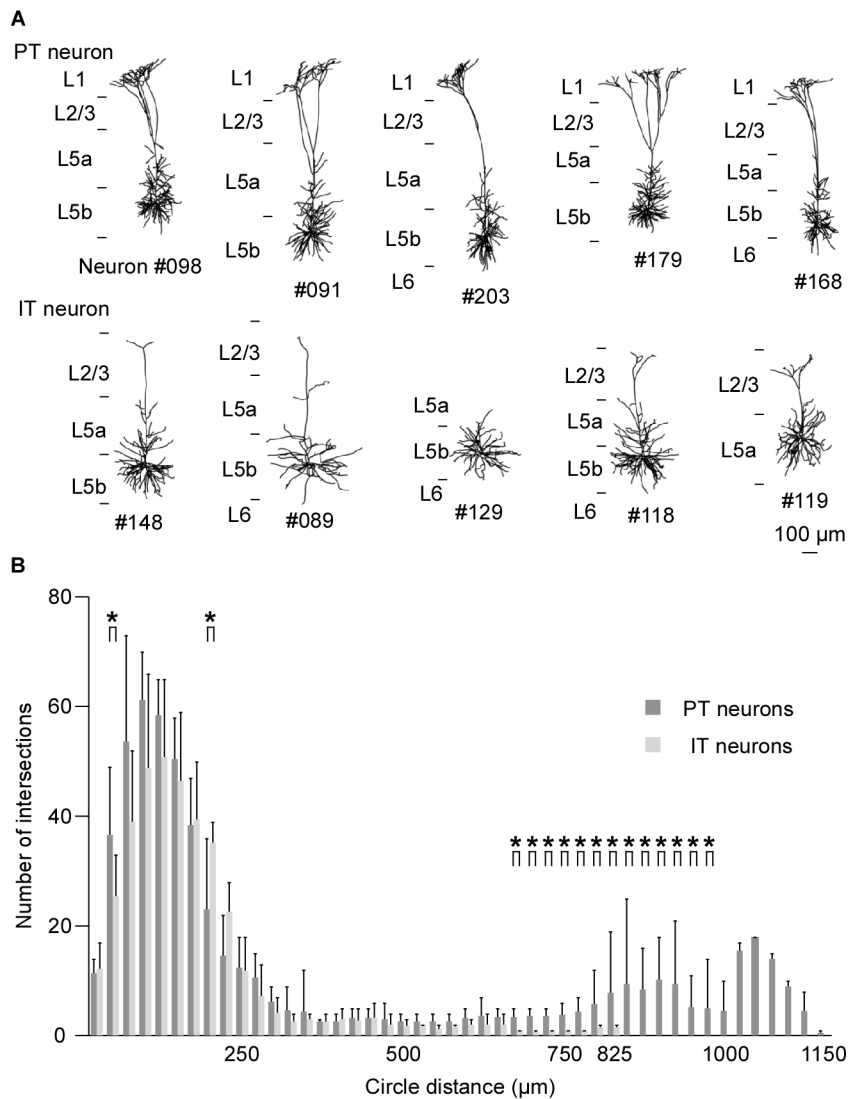


Figure 9. Dendrites and cell bodies of labeled PT and IT neurons. **A**, Reconstruction of dendrites and cell bodies of PT neurons (upper row) and IT neurons (lower row). **B**, The Sholl analysis revealed that PT neurons had more apical dendritic processes compared with IT neurons. Asterisks indicate statistically significant differences in the numbers of dendritic intersections between PT neurons and IT neurons ($p < 0.05$, Wilcoxon rank-sum test). The data are shown as mean and SD.